

Admixtures to d -wave gap symmetry in untwinned $\text{YBa}_2\text{Cu}_3\text{O}_7$ superconducting films measured by angle-resolved electron tunneling

H.J.H. Smilde, A.A. Golubov, Ariando, G. Rijnders, J.M. Dekkers,
S. Harkema, D.H.A. Blank, H. Rogalla, and H. Hilgenkamp
Faculty of Science and Technology and MESA⁺ Research Institute,
University of Twente, P.O. Box 217, 7500 AE Enschede, The Netherlands
(Dated: November 13, 2018)

We report on an ab -anisotropy of $J_{c\parallel b}/J_{c\parallel a} \cong 1.8$ and $I_c R_{n\parallel b}/I_c R_{n\parallel a} \cong 1.2$ in ramp-edge junctions between untwinned $\text{YBa}_2\text{Cu}_3\text{O}_7$ and s -wave Nb. For these junctions, the angle θ with the $\text{YBa}_2\text{Cu}_3\text{O}_7$ crystal b -axis is varied as a single parameter. The $R_n A(\theta)$ -dependence presents 2-fold symmetry. The minima in $I_c R_n$ at $\theta \cong 50^\circ$ suggest a real s -wave subdominant component and negligible d_{xy} -wave or imaginary s -wave admixtures. The $I_c R_n(\theta)$ -dependence is well-fitted by 83% $d_{x^2-y^2}$ -, 15% isotropic s - and 2% anisotropic s -wave order parameter symmetry, consistent with $\Delta_b/\Delta_a \cong 1.5$.

PACS numbers: 74.20.Rp, 74.50.+r, 74.72.Bk, 74.78.Bz, 85.25.-j

Phase-sensitive experiments^{1,2} and tunnel spectroscopy³ have provided rich evidence for the sign change of the pair wave function in the crystal ab -plane of high- T_c superconductors. Insight in the extent of subdominant admixtures to the $d_{x^2-y^2}$ -wave symmetry is less well established. They are of high importance for the basic understanding of high- T_c superconductivity and the design of novel d -wave based Josephson devices, but also for standard high- T_c junctions. They determine for instance the exact position of the nodes, and the amount of ab -anisotropy.

In $\text{YBa}_2\text{Cu}_3\text{O}_7$ strong anisotropy in the electronic structure has been reported, which can be interpreted as an effective mass anisotropy along the a - and b -axes: An elongated vortex shape by scanning tunneling spectroscopy⁴ suggests 50% anisotropy. Sixty percent anisotropy is found in the London penetration depth by far-infrared spectroscopy,⁵ as well as using c -axis $\text{YBa}_2\text{Cu}_3\text{O}_7/\text{Pb}$ Josephson junctions with a magnetic field oriented parallel to the a - or b -axis.⁶ Other studies, neutron scattering on flux-line lattices⁷ and single crystal torque-measurements,⁸ indicate a smaller anisotropy of 1.2. Related, surface impedance⁹ and resistivity measurements¹⁰ demonstrate an anisotropy of $R_{s\parallel a}/R_{s\parallel b} \approx 1.5$ to 1.6 and $\sqrt{\rho_a/\rho_b} \approx 1.5$ respectively.

Also, implications for the anisotropy of the superconducting gap have been discussed. Raman scattering¹¹ evidences a real isotropic s -wave admixture of 5%; thermal conductivity measurements in a rotating magnetic field¹² place a maximum of 10% based on the node positions. Angle-resolved photoemission spectroscopy (ARPES)¹³ indicates larger ab -anisotropy of $\Delta_b/\Delta_a = 1.5$. The use of untwinned single-crystals is considered crucial in all these studies. However, clear consensus on subdominant order parameter symmetries is not reached, nor is detailed angle-resolved data in the ab -plane of thin films available, although first attempts on twinned films have been performed.¹⁴ In view of this, we present here new results on the anisotropy, comparing untwinned and twinned $\text{YBa}_2\text{Cu}_3\text{O}_7$.

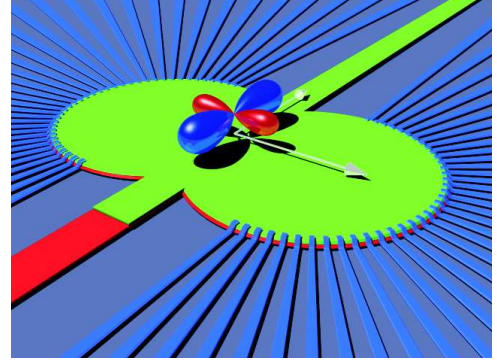


FIG. 1: (Color online) Angle-resolved electron tunneling with $\text{YBa}_2\text{Cu}_3\text{O}_7/\text{Au}/\text{Nb}$ ramp-type junctions oriented every 5° over 360° . The $\text{YBa}_2\text{Cu}_3\text{O}_7$ base-electrode (red) is covered by SrTiO_3 insulator (green), and contacted by a Au barrier (not visible) and a Nb counter-electrode (blue). The arrows (white) indicate the main crystal orientations in the ab -plane of the high- T_c superconducting material.

In untwinned $\text{YBa}_2\text{Cu}_3\text{O}_7$ thin films, the usual ‘random’ exchange of the a - and b -axis is eliminated. This enables to study the electronic properties angle-resolved in the ab -plane. The experimental layout is summarized in Fig. 1. Basically, the $\text{YBa}_2\text{Cu}_3\text{O}_7$ base-electrode is patterned into a nearly circular polygon, changing the orientation from side to side by 5 degrees. A Au barrier and Nb counter-electrode contact each side. In this way, the angle with respect to the (010)-orientation is varied as a single parameter.

First, bilayers of 170 nm $\text{YBa}_2\text{Cu}_3\text{O}_7$ and 100 nm SrTiO_3 are grown by pulsed-laser deposition (PLD) on single-crystal SrTiO_3 substrates. The $\text{YBa}_2\text{Cu}_3\text{O}_7$ films are optimally doped, with $T_{c,0} \geq 89$ K. Ramps are ion-milled in the bilayers using a photo resist stencil. To assure equivalent ramp quality over 360° , the sample stage is rotated around the substrate normal, while maintaining the angle of incidence of the Ar-ion beam constant at 40° with the substrate plane. The resulting ramp-angle

	twinned	untwinned
SrTiO ₃ : α/β	0.12°/119.0°	1.07°/357.9°
YBa ₂ Cu ₃ O ₇ : α/β	0.20°/97.3°	0.75°/346.3°
a	3.866(3)	3.849(6)
Cell Par. (Å) b	3.867(4)	3.892(7)
c	11.678(3)	11.703(7)

TABLE I: Vicinal angle α and its orientation β of the SrTiO₃ substrates and YBa₂Cu₃O₇ films. The YBa₂Cu₃O₇ data is obtained after device completion.

with the substrate plane is $\alpha_R \cong 30^\circ$. On a microscopic scale the interfaces may present some faceting, albeit less than in e.g. grain boundaries. This faceting is not expected to affect the main conclusions of the presented studies. After removal of the photo-resist stencil and a short 90°-incidence ion-mill for cleaning purposes, a 5 nm YBa₂Cu₃O₇ interlayer¹⁵ is deposited to prepare an in-situ interface to a 30 nm Au barrier formed also by PLD. Then, a 160 nm thick Nb counter-electrode is dc-sputter deposited through a lift-off stencil. Special care is taken to obtain a clean Au/Nb interface by a 50 s rf-plasma etch just before Nb deposition. After lift-off, redundant Au and YBa₂Cu₃O₇ interlayer material is removed by Ar-ion milling. The junctions are 4 μm wide.

The twin behavior of (001)-YBa₂Cu₃O₇ films is influenced by the substrate vicinal angle α and its in-plane orientation β .¹⁶ Here, α is defined between the crystallographic and optical substrate-normal, and β describes the in-plane orientation with respect to the SrTiO₃ (100) crystal axis. The degree of twinning can be controlled from completely untwinned to the presence of four ab -orientations, varying α from $\sim 1.1^\circ$ to a small vicinal angle ($\sim 0.1^\circ$), where $\beta \cong 0^\circ$. For $\alpha \cong 1.1^\circ$, growth with the b -axis along the step-ledges is induced, and only one crystal orientation is present. On the contrary, 4 twin orientations are present for small vicinal angle substrates. The twin orientations have pair-wise their in-plane diagonal of the YBa₂Cu₃O₇ crystal aligned with each substrate diagonal, so that a - and b -axes and vice versa are arranged nearly in parallel.¹⁶ After completion of the device, the YBa₂Cu₃O₇ base-electrode is examined with X-ray diffraction (XRD). An average of the a and b unit cell dimensions is found for twinned films (see Table I). For untwinned films, the individual a and b unit cell parameters can be distinguished and are close to single-crystal values. Detailed hk -scans of the (0 $\bar{3}$ 4) reflections show 4 different orientations for YBa₂Cu₃O₇ films grown on small vicinal angle substrates (Fig. 2a), associated with the above-mentioned 4 twin orientations. For films grown on substrates with $\alpha \cong 1.1^\circ$ however, only one orientation is present (Fig. 2b).

The XRD and electrical data presented in this article correspond to the same samples. Figure 3 presents the electrical characterization of the twinned base-electrode sample (a-c), and the untwinned one (d-f,h). During the measurement, the magnetically shielded sample space re-

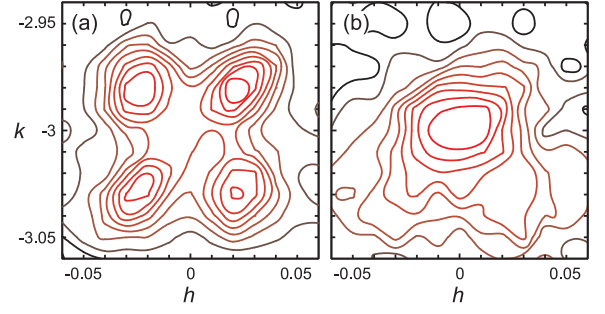


FIG. 2: (Color online) Logarithmic contour plots of hk -scans near the (0 $\bar{3}$ 4) reflection of YBa₂Cu₃O₇: (a) grown on a small vicinal angle SrTiO₃ substrate ($\alpha \approx 0.12^\circ$), and (b) grown on an $\alpha \cong 1.07^\circ$ and $\beta \cong -2.1^\circ$ vicinal SrTiO₃ substrate. Both scans are measured after device completion.

duces background fields below 0.1 μT . Trapped flux in or near the junctions is excluded by systematic $I_c(B)$ measurements, assuring a correctly determined critical current density (J_c). The superconducting properties of the Au/Nb bilayer are independent of the orientation. Therefore, J_c depends on the in-plane orientation θ with respect to the b -axis of the YBa₂Cu₃O₇ crystal only, and presents four maxima for both samples, approaching zero in between. This is in agreement with predominant $d_{x^2-y^2}$ -wave symmetry of the superconducting wave function in one electrode only, and a $\cos(2\theta)$ -dependence is expected.¹⁷ In closer detail, the nodes of the untwinned YBa₂Cu₃O₇ sample are found at 5° from the diagonal between the a - and b -axis. This presents direct evidence for a significant real isotropic s -wave admixture. A first estimate for the s - over $d_{x^2-y^2}$ -wave gap-ratio is calculated as $|\cos(2\theta_0)| \cong 17\%$ for a node angle $\theta_0 = 50^\circ$. For the twinned base-electrode, the nodes are found at the diagonal, which is expected if all twin orientations are equally present, and contributions of subdominant components average out to zero.

The suppressed J_c in the nodal direction ($\leq 0.01 J_{c\parallel(010)}$) suggests small, if not absent, imaginary admixtures,¹⁸ for instance of isotropic is -wave or id_{xy} -wave type which in contrast would lift the nodes. A significant real d_{xy} -wave admixture is excluded, because this would induce a rotation in the same direction with respect to the crystal of all nodes.

In the untwinned case, the J_c -value is 1.8 times larger in the b - than in the a -direction. Preparation effects can be eliminated, since circular symmetry with respect to the substrate normal has been conserved at all phases of the fabrication. The normal-state resistance ($R_n A$) is lower along the b - than along the a -axis, and presents a two-fold symmetry axis for the untwinned case. Using the angle-resolved values, the anisotropy in the $I_c R_n$ -product amounts to $I_c R_{n\parallel b} / I_c R_{n\parallel a} \cong 1.22$.

To estimate the $I_c R_n$ -products in our junctions, we model them as SINS' structures, where S is YBa₂Cu₃O₇, I is the YBa₂Cu₃O₇/Au interface barrier, which has much higher resistance than the Au (N) and the Au/Nb

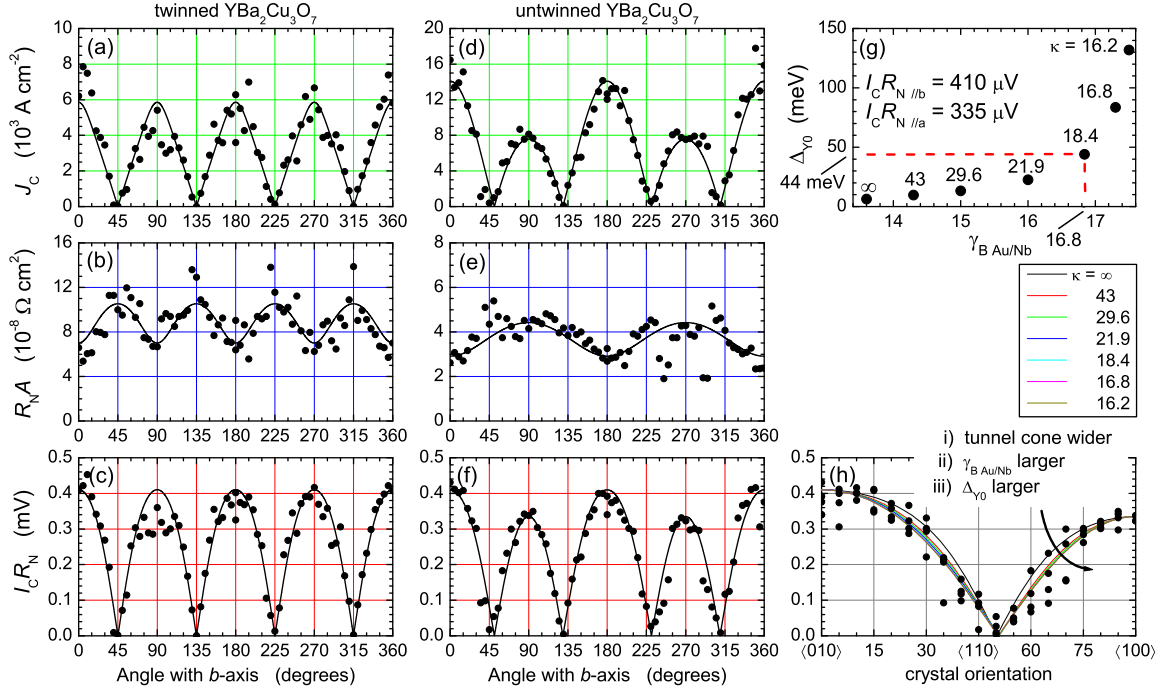


FIG. 3: (Color online) J_c , $R_n A$, and $I_c R_n$ -product vs the junction orientation with respect to the YBa₂Cu₃O₇ crystal for twinned (a-c), and untwinned (d-f,h) YBa₂Cu₃O₇ at $T = 4.2$ K and in zero magnetic field. (see text for description fits) (g) Fit parameter evolution for untwinned case, and (h) corresponding fits.

(N/S') interface. From independent resistance measurements on our PLD Au ($\rho_{Au} \cong 4.6 \mu\Omega$ cm at 4.2 K), the mean-free-path is $l_{Au} \cong 18$ nm, and the dirty-limit coherence length is $\xi_{Au} \cong 49$ nm. Using these values and the YBa₂Cu₃O₇/Au interface resistance $R_{BY/Au} \geq 10^{-8} \Omega$ cm², the transparency at this interface is low: $\gamma_{BY/Au} \geq 440$, where $\gamma_B = R_{BY/Au}/\rho_{Au}\xi_{Au}$.¹⁹ From a small Fermi-velocity mismatch, we estimate the Au/Nb interface transparency much larger, $\gamma_{BAu/Nb} < 20$. The electrode-separation is $d_{Au} = 26$ nm for 30 nm thick Au and ramp angle $\alpha_R = 30^\circ$. Since $l_{Au} < d_{Au}$ and $l_{Au} < \xi_{Au}$, Au is in the diffusive regime, while YBa₂Cu₃O₇ is in the clean limit with the anisotropic gap function Δ_Y .

We extend the expression for the supercurrent in diffusive SINS' structures¹⁹ to our case of a low-transparent junction between a clean d -wave superconductor and a diffusive NS' bilayer. The contribution of midgap Andreev bound states is small in such a junction²⁰ and can be neglected.

$$I_s R_n = \frac{1}{N} \iint d\phi d\chi \sin(\chi) D \gamma \sin(\Delta\varphi) \quad (1)$$

$$\gamma = \frac{2\pi k_B T}{e} \sum_{n=0}^{\infty} \frac{\Phi \Delta_Y}{\sqrt{\Phi^2 + \omega_n^2} \sqrt{\Delta_Y^2 + \omega_n^2}} \quad (2)$$

$$\Phi = \frac{\pi k_B T_{cNb} \Delta_{Nb}}{\pi k_B T_{cNb} + \gamma_{BAu/Nb} (d_{Au}/\xi_{Au}) \sqrt{\Delta_{Nb}^2 + \omega_n^2}} \quad (3)$$

Here χ is the angle with the interface normal, and $N = \iint d\phi d\chi \sin(\chi) D$ is the normalization constant. The integration is performed over angles $\phi = 0$ to 2π , and $\chi = 0$ to $\frac{\pi}{2}$ of a half-sphere of all trajectories: for each junction orientation, and taking the crystal orientation and ramp-angle into account. The barrier transmission coefficient $D = \cos(\chi) \exp[\kappa\{1 - \cos^{-1}(\chi)\}]$ is in the limit of a small YBa₂Cu₃O₇ Fermi velocity, where κ describes the tunnel-cone size. The sum in Eq.(2,3) is taken over the Matsubara frequencies $\omega_n = \pi T(2n + 1)$. Δ_Y is the anisotropic gap function in YBa₂Cu₃O₇, and Φ is the isotropic proximity-induced gap function in Au. Δ_{Nb} and T_{cNb} are the bulk pair potential and the critical temperature of Nb, respectively. The critical current I_c and $I_c R_n$ -product should be found by calculating a maximum of $I_s R_n$ over the phase difference $\Delta\varphi$ across the junction.

Tunneling along the a - and b -axis may then be compared theoretically in terms of the ratio $\Gamma = I_c R_{n\parallel b}/I_c R_{n\parallel a}$. Using Eqs.(1-3), it can be shown that for constant properties of the Nb/Au bilayer, the ratio of the YBa₂Cu₃O₇ gap for these directions is $\Delta_{Y\parallel b}/\Delta_{Y\parallel a} \geq \Gamma$. Therefore, the observed anisotropy of $\Gamma \cong 1.22$ represents a lower limit for this gap ratio, which is valid for extremely small ratios $\Delta_Y/\Delta_{Nb} \ll 0.1$. For increasing ratio Δ_Y/Δ_{Nb} , the value $\Gamma \cong 1.22$ requires a rapid increase of $\Delta_{Y\parallel b}/\Delta_{Y\parallel a}$. In this estimate, Γ depends only on the gap ratios and on the Au/Nb interface transparency.

The anisotropic gap in YBa₂Cu₃O₇ depends on the in-plane angle θ (0 to 2π), and the angle η ($-\frac{\pi}{2}$ to $\frac{\pi}{2}$) with the ab -plane. Various possible symmetry functions exist to

describe this gap. Here, we consider the following 3D gap function in $\text{YBa}_2\text{Cu}_3\text{O}_7$ consisting of a dominant $d_{x^2-y^2}$ -wave component with an isotropic and an anisotropic s -wave admixture:

$$\Delta_Y = \Delta_{Y_0} \cos^2(\eta) \sum_{i=0}^2 c_i \{ \cos^2(\theta) - \sin^2(\theta) \}^i \quad (4)$$

with the coefficients $c_1 > c_0, c_2$ and $c_1 + c_0 + c_2 = 1$. Here Δ_{Y_0} denotes the magnitude of the $\text{YBa}_2\text{Cu}_3\text{O}_7$ gap at the interface. Consistent with our earlier estimate $\Delta_{Y\parallel b}/\Delta_{Y\parallel a} > 1.22$, the gap-ratio is taken as $\Delta_{Y\parallel b}/\Delta_{Y\parallel a} \cong 1.5$ in agreement both with the observed node positions and ARPES.¹³ With this, the coefficients are found from the fit to the data $c_0 = 0.15$, $c_1 = 0.83$ and $c_2 = 0.02$. Other choices for the gap symmetry functions lead to slightly different numbers but will not alter the basic results of our calculations.

A series of fits is presented in Fig. 3h: the wider the tunneling cone (smaller κ), the smaller is the width of the oscillations in the $I_c R_n(\theta)$ -dependence (arrow). The effective $\text{YBa}_2\text{Cu}_3\text{O}_7$ gap Δ_{Y_0} and $\gamma_{B_{Au/Nb}}$ must then become larger. This dependence is presented in Fig. 3g. The minimum value Δ_{Y_0} occurs for normal-incidence tunneling ($\lim \kappa \rightarrow \infty$), so that $\Delta_{Y_0} \geq 6.4$ meV. For reasonable Δ_{Y_0} values (< 0.5 eV), $\gamma_{B_{Au/Nb}}$ varies from 13.6 to about 18. This gives an estimate for the Au/Nb interface resistance: $R_B A \cong 0.36 \pm 0.05$ $n\Omega$ cm^2 . In contrast to $\gamma_{B_{Au/Nb}}$, it is not possible to give an accurate estimate for the $\text{YBa}_2\text{Cu}_3\text{O}_7$ gap from our data. Therefore, we choose to fit the data with $\Delta_{Y_0} = 44$ meV, $\gamma_{B_{Au/Nb}} = 16.8$ in Figs. 3c and 3f. These are not claimed to be the correct values; the simulation demonstrates however that large Δ_{Y_0} may well be consistent with small $I_c R_n$ values. For the untwinned case $\kappa = 18.4$, corresponding to a tunnel cone with a full-width-half-maximum (FWHM) of 31.0° (cosine-term of D not included). For the twinned case, the $I_c R_n(\theta)$ -dependence is simulated with the same parameters, except for a slightly smaller cone ($\kappa = 26.3$, FWHM = 26.0°), and assuming equal presence of both twin orientations: $\frac{1}{2}[I_c R_n(\theta) + I_c R_n(\theta + \frac{\pi}{2})]$. The smaller tunnel cone for the twinned case is consistent with higher $R_n A$ - and lower J_c -values. This may result from a slightly thicker tunnel barrier at the $\text{YBa}_2\text{Cu}_3\text{O}_7/\text{Au}$ interface, e.g., due to minor variations in the Au PLD-conditions, modifying this interface.

The $R_n A(\theta)$ -dependence is fitted with an ellipsoidal relation of the conductivity projections along the main

crystal directions of the $\text{YBa}_2\text{Cu}_3\text{O}_7$. Written in terms of the $R_n A$ -values along these directions, this gives $R_n A(\theta) = \sqrt{R_n A_{\parallel b}^2 \cos^2(\theta) + R_n A_{\parallel a}^2 \sin^2(\theta)}$. Fig. 3e shows the result using $R_n A_{\parallel a} = 44$ $n\Omega$ cm^2 and $R_n A_{\parallel b} = 29$ $n\Omega$ cm^2 . For the twinned case, a geometrical average of the conductivities is assumed, $R_n A(\theta) = 2/[R_n A^{-1}(\theta) + R_n A^{-1}(\theta + \frac{\pi}{2})]$. The used values in Fig. 3b read $R_n A_{\parallel a} = 141$ $n\Omega$ cm^2 , $R_n A_{\parallel b} = 47$ $n\Omega$ cm^2 . Although these phenomenological fits are indicative, angle-resolved calculations including aspects of the $\text{YBa}_2\text{Cu}_3\text{O}_7$ band-structure and band-bending effects are needed for a detailed understanding. Finally, the $J_c(\theta)$ fits are obtained with the ratios of the $I_c R_n(\theta)$ - and the $R_n A(\theta)$ -dependencies, the ensemble of which gives a consistent simulation of the angle-resolved junction properties.

The experimental results support theories based on a 2-band model of the chains and planes^{21,22} modeled with a symmetric, anti-symmetric and isotropic component. Furthermore, our findings agree with c -axis tunneling from two twinned $\text{YBa}_2\text{Cu}_3\text{O}_7$ grains to a Pb counter-electrode that depends on the magnetic field orientation,²³ and angle-dependence studies on grain boundary junctions.²⁴ For all-high- T_c junctions and circuits, we mark the anisotropy as a possible intrinsic source of their limited reproducibility: both twin orientations may not be uniformly present, yielding an important variation in J_c . Control over the crystal orientation then presents a key to improvement. Another important aspect concerns the nodes at 5° from the $\langle 110 \rangle$ crystal direction. The best choice for the electrode-orientation of devices aiming a d -wave induced second harmonic in the current-phase relation, such as $\frac{\pi}{2}$ -SQUIDs based on grain boundary junctions, may therefore deviate from the $\langle 110 \rangle$ crystal direction.

In conclusion, an angle-resolved electron tunneling study using Josephson junctions with an untwinned $\text{YBa}_2\text{Cu}_3\text{O}_7$ base-electrode is presented. Evidence for significant in-plane anisotropy in the electronic properties of $\text{YBa}_2\text{Cu}_3\text{O}_7$ is found.

The authors thank M. Yu. Kupriyanov, J. R. Kirtley, C. C. Tsuei, C. W. Schneider and J. Mannhart for valuable discussions. This work is supported by the Dutch Foundation for Research on Matter (FOM), and the Netherlands Organization for Scientific Research (NWO).

¹ D. A. Wollmann *et al.*, Phys. Rev. Lett. **71**, 2134 (1993).

² C. C. Tsuei *et al.*, Phys. Rev. Lett. **73**, 593 (1994).

³ J. Y. T. Wei *et al.*, Phys. Rev. Lett. **81**, 2542 (1998).

⁴ I. Maggio-Aprile *et al.*, Phys. Rev. Lett. **75**, 2754 (1995).

⁵ D. N. Basov *et al.*, Phys. Rev. Lett. **74**, 598 (1995).

⁶ A. G. Sun *et al.*, Phys. Rev. B **52**, R15731 (1995).

⁷ S. T. Johnson *et al.*, Phys. Rev. Lett. **82**, 2792 (1999).

⁸ T. Ishida *et al.*, Physica C **263**, 260 (1996).

⁹ K. Zhang *et al.*, Phys. Rev. Lett. **73**, 2484 (1994).

¹⁰ T. A. Friedmann *et al.*, Phys. Rev. B **42**, 6217 (1990).

¹¹ M. F. Limonov *et al.*, Phys. Rev. Lett. **80**, 825 (1998).

¹² H. Aubin *et al.*, Phys. Rev. Lett. **78**, 2624 (1997).

¹³ D. H. Lu *et al.*, Phys. Rev. Lett. **86**, 4370 (2001).

¹⁴ D. J. van Harlingen *et al.*, Physica C **317-318**, 410 (1999).

- ¹⁵ H. J. H. Smilde *et al.*, Appl. Phys. Lett. **80**, 4579 (2002).
- ¹⁶ J. M. Dekkers *et al.*, Appl. Phys. Lett. **83**, 5199 (2003).
- ¹⁷ M. Sigrist, T. M. Rice, J. Phys. Soc. Jpn. **61**, 4283 (1992).
- ¹⁸ D. J. van Harlingen, Rev. Mod. Phys. **67**, 515 (1995).
- ¹⁹ A. A. Golubov *et al.*, Phys. Rev. B **51**, 1073 (1995).
- ²⁰ R. A. Riedel, P. F. Bagwell, Phys. Rev. B **57**, 6084 (1998).
- ²¹ I. I. Mazin, A. A. Golubov, A. D. Zaikin, Phys. Rev. Lett. **75**, 2574 (1995).
- ²² C. O'Donovan *et al.*, Phys. Rev. B **55**, 9088 (1997).
- ²³ K. A. Kouznetsov *et al.*, Phys. Rev. Lett. **79**, 3050 (1997).
- ²⁴ F. Lombardi *et al.*, Phys. Rev. Lett **89**, 207001 (2002).